Paleoclimate controls on lithium enrichment in Great Basin Pliocene-Pleistocene lacustrine clays

Catherine A. Gagnon[1,2,†], Kristina L. Butler[3], Elizabeth Gaviria[1,4], Alexa Terrazas[5], Annabelle Gao[1], Tripti Bhattacharya[6], David F. Boutt[7], Lee Ann Munk[8], Daniel E. Ibarra[1,2]

[1]*Department of Earth, Environmental and Planetary Science, Brown University, Providence, RI 02912, USA*
[2]*Institute at Brown for Environment and Society, Brown University, Providence, RI 02912, USA*
[3]*Department of Geological Sciences, Jackson School of Geosciences, University of Texas at Austin, Austin, TX 78712, USA*
[4]*Department of Earth, Environmental and Planetary Sciences, Rice University, Houston, TX 77005, USA*
[5]*Department of Ocean and Atmospheric Sciences, University of California, Los Angeles, CA, 90095, USA*
[6]*Department of Earth Sciences, Syracuse University, Syracuse, NY 12344, USA*
[7]*Department of Geosciences, University of Massachusetts-Amherst, Amherst, MA 01003, USA*
[8]*Department of Geological Sciences, University of Alaska Anchorage, Anchorage, AK 99508, USA*

This manuscript has been submitted to *GSA Bulletin*. This paper is a non-peer reviewed preprint submitted to *EarthArXiv*. Subsequent version of this manuscript may have different content.

Paleoclimate controls on lithium enrichment in Great Basin Pliocene-Pleistocene lacustrine clays

Catherine A. Gagnon[1,2,†], Kristina L. Butler[3], Elizabeth Gaviria[1,4], Alexa Terrazas[5], Annabelle Gao[1], Tripti Bhattacharya[6], David F. Boutt[7], Lee Ann Munk[8], Daniel E. Ibarra[1,2]

[1]*Department of Earth, Environmental and Planetary Science, Brown University, Providence, RI 02912, USA*

[2]*Institute at Brown for Environment and Society, Brown University, Providence, RI 02912, USA*

[3]*Department of Geological Sciences, Jackson School of Geosciences, University of Texas at Austin, Austin, TX 78712, USA*

[4]*Department of Earth, Environmental and Planetary Sciences, Rice University, Houston, TX 77005, USA*

[5]*Department of Ocean and Atmospheric Sciences, University of California, Los Angeles, CA, 90095, USA*

[6]*Department of Earth Sciences, Syracuse University, Syracuse, NY 12344, USA*

[7]*Department of Geosciences, University of Massachusetts-Amherst, Amherst, MA 01003, USA*

[8]*Department of Geological Sciences, University of Alaska Anchorage, Anchorage, AK 99508, USA*

† Corresponding author: catherine_gagnon@brown.edu

ABSTRACT

Terminal lakes are important archives of continental hydroclimate and in some cases contain important economic resources. Here we present an ~3.6 Myr lacustrine carbonate carbon and oxygen stable isotope record from a Great Basin continental drill core. We pair these measurements with bulk lithium concentrations to reveal a relationship between past climate and lithium enrichment in authigenic lacustrine clays. Further, we explore the possible effects of changing seasonality on the isotope record through the use of paired air mass trajectories and modern isotope data. Our findings show the evolution of the basin's moisture balance over million-year timescales, which we attribute to variations in precipitation seasonality as well as fluctuations in the amount of evaporation associated with changes in atmospheric moisture convergence and divergence. We observe a positive correlation between the oxygen isotope values of the lake carbonate and the bulk sediment lithium concentrations, which we argue is indicative of evapoconcentration of the lake environment and subsequent enrichment of the authigenic clays. Our results suggest a link between past hydroclimate changes and the formation of lithium rich authigenic clays feeding high lithium concentrations in this modern brine aquifer system.

INTRODUCTION

Evidence from the relatively recent geologic past suggests that the Great Basin region of the western United States experienced enhanced moisture convergence in both warmer and colder climates compared to the modern (Matsubara and Howard, 2009; Salzmann et al., 2011; Pound et al., 2014; Ibarra et al., 2014; 2018; Lee et al., 2021; Fu et al., 2021). For example, the Last Glacial Maximum (LGM) was a vastly different climate state, with global sea level 140 m lower and global

mean annual temperatures ~6 ºC cooler than present (Clark et al., 2009; Annan and Hargreaves, 2013; Lora and Ibarra, 2019). During this time, the Great Basin sustained many pluvial lakes whose maximum extents represent a balance between precipitation and evaporative demand and suggest a much wetter environment (Mifflin and Wheat, 1979; Reheis, 1999; Orme, 2008; Kurth et al., 2011; Godsey et al., 2011; Munroe and Laabs, 2013; Ibarra et al., 2014; Reheis et al., 2014; Oster and Ibarra, 2018; Santi et al., 2020). A metric for evaluating the moisture balance of these pluvial lakes is precipitation minus evaporation (P-E), associated with regional atmospheric convergence changes (e.g., Lora and Ibarra, 2019), which we will use hereafter when talking about moisture balance. Similarly, the mid-Pliocene (3-3.3 Ma) experienced wetter-than-modern conditions in the southwestern United States (Pound et al., 2014; Ibarra et al., 2018; Fu et al., 2022). However, and in contrast to the LGM, a combination of proxies and modeling efforts suggest the mid-Pliocene global mean annual temperature was around 3.5°C warmer than today and had atmospheric CO_2 levels greater than pre-industrial (Ravelo et al., 2004; Dowsett and Gill, 2010; Burke et al., 2018; Haywood et al., 2020). There are numerous hypotheses which have been invoked to explain the wet conditions in the mid-Pliocene. Burls and Fedorov (2017) propose that weaker atmospheric circulation in response to the different ocean surface temperature patterns of the Pliocene reduced meridional and zonal temperature gradients. Another recent hypothesis argues for more enhanced convergent monsoonal circulation that develops over late boreal summer due to increased SST in the Pliocene (Fu et al., 2022). Lastly, strengthened southwesterly moisture delivery could have resulted in greater wintertime precipitation that fed the southwest USA lakes (Ibarra et al., 2018).

Lake basins in the Great Basin are important archives of climate, and in some cases, they also host significant economic resources (e.g., Davis and Gleason 1986; Munk et al., 2011; Bradley et al., 2013; Castor and Henry, 2020). Clayton Valley Nevada is a long-lived Pliocene-Pleistocene

lake system and is also the location of the largest lithium brine resource in North America (Coffey et al., 2021). The availability of lithium is critical for the transition to renewable energy and electric vehicles because it is an important component of modern battery technology (e.g., Munk et al., 2016; Manthiram, 2017). In this study, sediment cores from Clayton Valley allow us the opportunity to explore the intersection between Pliocene-Pleistocene hydroclimate change and the formation of this important resource. Additionally, the similarity between the climate state of the mid-Pliocene and today (Burke et al., 2018; Haywood et al., 2020), with minimal changes in continental configuration, orography and paleogeography, make this lake system an excellent case study for how regional hydroclimate in the southwestern United States might evolve in the future. As such, in this study we address the following two key questions: *(1) How has the hydroclimate of Clayton Valley varied from the Pliocene-Pleistocene? (2) What role does climate play in the formation of lithium rich clays in the Clayton Valley Basin?*

To answer these questions we present a new carbonate-based stable isotope hydroclimate record for Clayton Valley (CV) a terminal basin in the Great Basin area of the western United States, and demonstrate through additional geochronology (cf. Coffey et al., 2021) that this basin contains lake deposits from the Pliocene to late Pleistocene. We measured, in detail, stable carbon and oxygen isotopes of carbonates from one of the previously described sediment cores (EXP2), and expand on the sedimentological interpretations of Coffey et al. (2021) to include thin section analysis and chemical weathering indices of alteration (CIA) based on bulk elemental analyses, as well as additional higher-resolution bulk lithium concentration measurements. Further, to provide a clear picture of the modern hydroclimate dynamics, we also include air mass back trajectory and analysis of precipitation for Clayton Valley using Hybrid Single-Particle Lagrangian Integrated Trajectory model (HYSPLIT) (Stein et al., 2015; Warner,

2018). We characterize these trajectories with nearby modern precipitation isotope data. Our results demonstrate that the long-term Pliocene to late Pleistocene hydroclimate evolution from wet deep-lake conditions to increasingly desiccated and punctuated pluvial lake conditions greatly influenced lithium accumulation in this lacustrine clay deposit, which are the primary source of lithium to the modern brine aquifer system.

SETTING

CV is a topographically closed half-graben basin in Esmeralda County along the western margin of the Basin and Range Province about 80 miles to the northwest of Death Valley (Fig. 1). Basement fault blocks of Late Neoproterozoic to Ordovician North American western passive margin siliciclastic and carbonate units bound the basin on all sides. Surficial deposits consist of Tertiary volcanic and sedimentary rocks. During the late Paleozoic and Mesozoic the region underwent shortening and low grade-metamorphism. Since ~16 Ma the area has undergone continuous extension (Coffey et al., 2021; Oldow et al., 2009; Burrus, 2013).

CV sits on the northernmost extent of the North American Monsoon (NAM) (e.g., Ray et al, 2007; Means, 2013; Bhattacharya et al., 2017). The average annual precipitation the area receives is 13 cm (Munk and Chamberlain, 2011), which is delivered in the summer months via the NAM and wintertime westerlies. The valley floor playa spans 100 km^2 at an elevation of 1298 m. The entire topographic watershed for Clayton Valley is 1,437 km^2 (Coffey et al., 2021). Recent groundwater flow modeling has shown a potential contribution of surrounding basins of upwards to 12,610 km^2 (Brooks et al., 2014; Underdown et al, 2017). Despite the large influence of interbasin flow, the groundwater terminates from all surrounding basins into Clayton Valley

(Rush, 1968; Coffey et al., 2021). Water outflow is therefore limited to playa evaporation and evapotranspiration in the lowland areas of the valley where there is a shallow groundwater table.

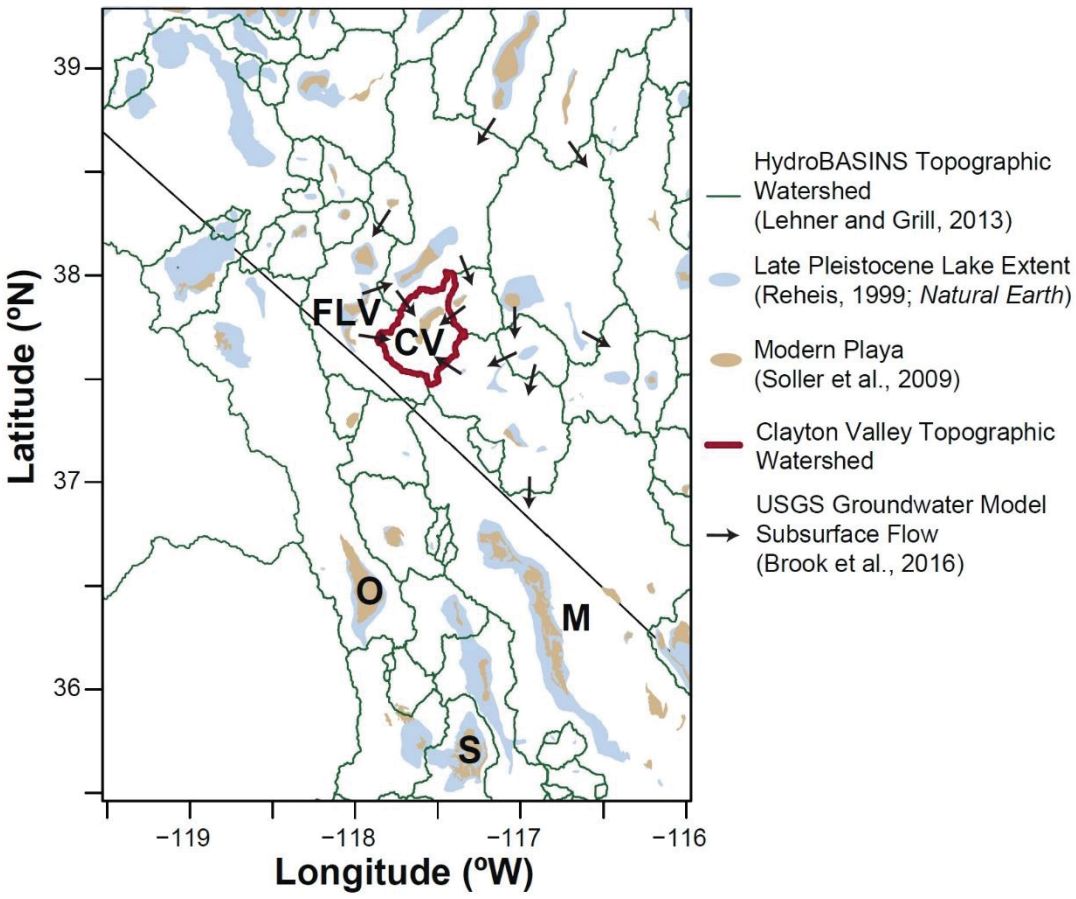

Figure 1. Map of Clayton Valley (CV), Fish Lake Valley (FLV), Lake Manly (M), Searles Lake (S), and Owens Valley (O) with watershed boundaries, late Pleistocene lake extents and modern playas. Note that the groundwater flow vectors (Brook et al., 2016) surrounding the study site terminate in the CV basin.

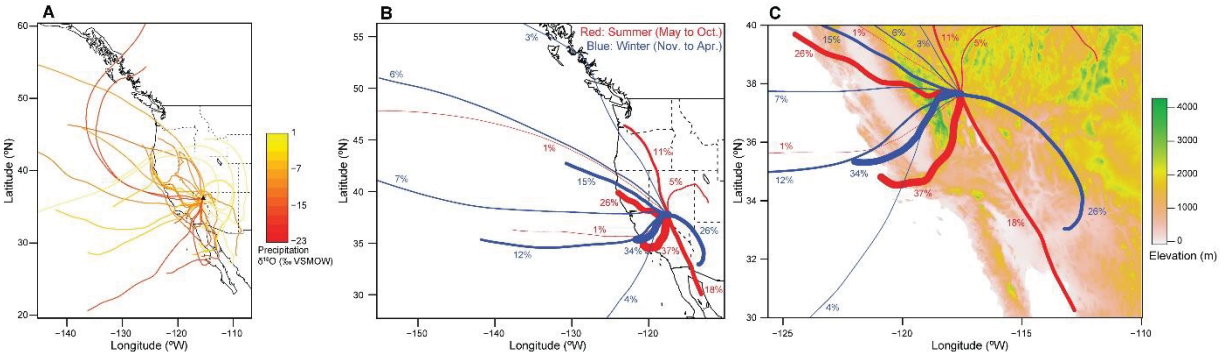

Figure 2. (A) Annual average 3-day air mass back trajectories for Las Vegas weighted by precipitation. Colors indicate modern precipitation isotope values (Welker, 2012) recorded in Las Vegas, NV. (B) Average winter (blue) and summer (red) 3-day air mass back trajectories for CV weighted by precipitation. (C) as in (B) zoomed in with elevation.

MATERIALS AND METHODS

The EXP2 core was one of five cores drilled in the CV basin between June 2017 and November 2017 by the Albemarle Corporation. The 3,250 ft (990.6 meter) long core was photographed and logged to the nearest tenth of a foot, with depths herein converted to meters. Coffey et al. (2021) detailed the sedimentology producing the stratigraphic column shown in Figure 3. The dominant sedimentology from 0-47.24 m consists of sands and gravels. From 47.24 m to about 243.54 m the material is composed of silts and finer-grained sands. From 243.54-405.38 m there are predominately greenish gray clays with some thinly-bedded ashes. From 405.38 m-534.92 the clays are interbedded with halite beds up to 8 meters thick. From 534.92-768.10 m the sediments are predominantly greenish gray clay with the occasional thin-bedded ashes. From 768.10 m- 894.59 m the material is silt. The remaining base of the core is angular gravel derived from a partially lithified tuff sitting atop basement rock.

In the following we briefly summarize our methods. We evaluated oriented thin sections under an optical microscope to assess the degree of alteration of lake carbonates. We observed fine-grained micritic texture with little to no overgrowth on the carbonate grains and no large or small crosscutting calcite veins (Fig. 2), suggestive of primary lacustrine clays with little to no secondary precipitation. Whole rock and bulk lithium concentrations were analyzed by SGS Lakefield, as in Coffey et al. (2021). XRF analysis and mineral percentages from XRD (when available) were used to calculate weathering indices (corrected for carbonate content). We constructed a new age model using previously reported and new $^{40}Ar/^{39}Ar$ ages from volcanic ash sanidine and biotite crystals, and a new U-Pb age on zircon grains. We constructed a Monte-Carlo based age-depth model using six ages and one correlated ash age (Fig. 2) and assigned probable ages to all samples. An apparent change in sedimentation rate or a hiatus is observed near the base of the core at 775.11m and thus sample ages below this depth are assigned based on three possible scenarios (see supplementary material; Figure 3). The hydroclimate interpretations for CV relies heavily on the time evolution of oxygen and carbon isotopes along with the sedimentology of the core. A total of 285 carbonate samples from EXP2 were measured for $\delta^{18}O$ and $\delta^{13}C$. The stable isotope measurements were made on one of three instruments– Thermo Finnigan MAT 252 with a Kiel III at Brown University, Thermo Finnigan MAT 253+ with a Kiel IV at Brown University, or a Thermo Finnegan Deltaplus XL with a gasbench at Stanford University (Table 1), with replication across laboratories and mass spectrometers. Carbonate stable isotope ratios are reported using standard δ-notation relative to the VPDB standard. In addition to the isotope timeseries, we used HYSPLIT to create 3-day back-trajectories at 1500 meters above ground level for precipitation events at CV. We used 40 years of modern NARR (1979-2019) meteorological records, and geographically clustered the

precipitation trajectories, weighting them by frequency. Further detailed methods can be found in the supplementary material.

RESULTS AND DISCUSSION

Paleoenvironmental Interpretation of Clayton Valley

The stratigraphic succession of the EXP2 core is typical of an underfilled to balance-filled lake in an extensional basin setting (e.g., Carroll and Bohacs, 1999; Ingersoll, 2012). Assuming no hiatuses the sedimentation rate appears to be highest at the base of the core, where we observe gravel that fines upward into lacustrine clays. As such, we infer that the sedimentation rate is slower from 4,529 to 2,478 ka and is relatively linear, slightly faster, and unvarying from 2,478 to 22 ka to the top of the core.

Depositional System

Based on the sedimentology we describe the depositional system. Starting at ~3.5 Ma, CV sustained a deep lake, evident from the thick green laminated lacustrine muds which persisted intermittently until the late Pleistocene with the youngest lacustrine muds at ~17.6 ka. The thick halite beds that abruptly punctuate the lacustrine deposits likely represent rapid changes in the moisture balance for the CV area which operate on ten to hundred-year timescales, based on our linear age model, between ~1.4 to 1.8 Ma. This change in the moisture budget is also supported by a notable transition in the degree of weathering from high to low, such that we start to see less weathered material in the core above the halite section. At around 35 ka, the sediments coarsen upward in the section, signifying a gradual transition from a long-standing lake to the more arid playa environment, consistent with no significant LGM lake above

the playa being present in this basin (Reheis, 1999). The uppermost coarse-grained sediments in EXP2 are more difficult to interpret, due to the poor core recovery, so it is unclear when the playa lake became permanently desiccated, we infer this to be ~17.6 ka. Further, in the neighboring valley to the west, Fish Lake Valley (FLV), there is minimal evidence for a large LGM (~21 ka) lake (Reheis et al., 1993; Reheis, 1999a).

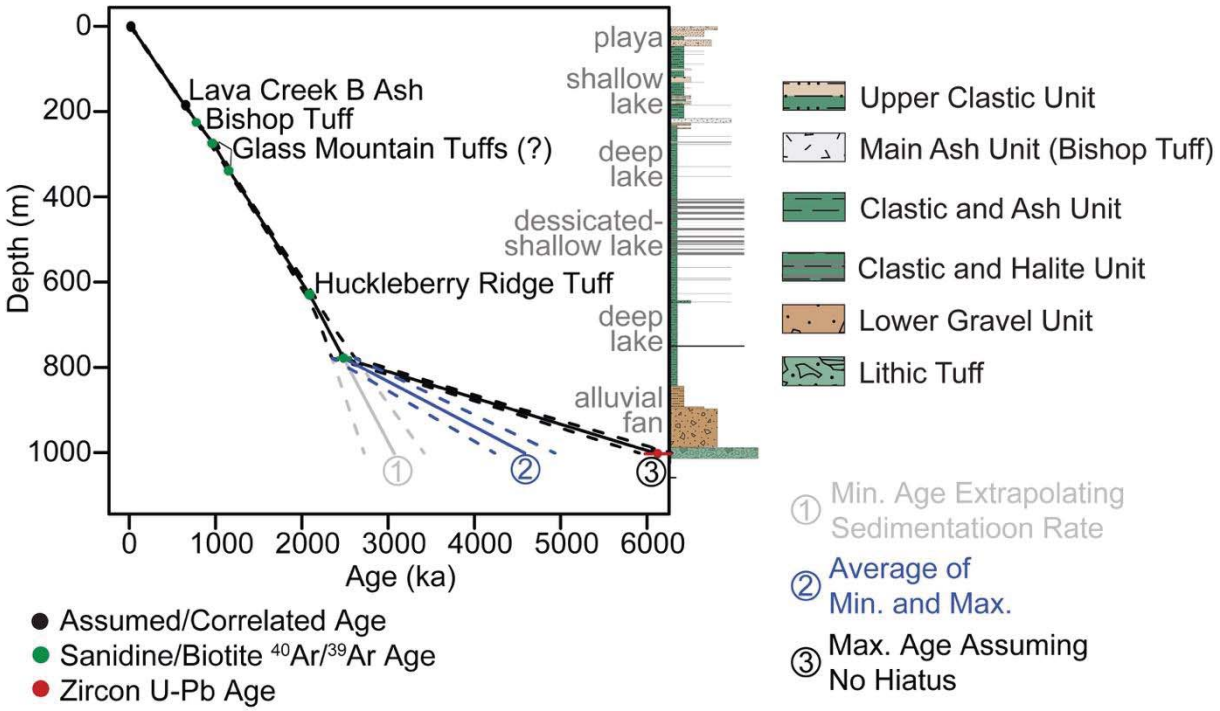

Figure 3. Age model for Clayton Valley EXP2 core alongside a stratigraphic column detailing the major lithologic units. Age model solid lines indicate mean ages, while dotted lines are 2σ based. Between the last two ages, we calculate (1) the linear interpolation assuming no hiatuses (black), (2) the projection of earlier sedimentation rates (gray), and (3) the average between these two (blue).

Stable Isotope Results

The $\delta^{18}O$ values range from -14.1‰ to +4.6‰. The $\delta^{13}C$ values range from -8.0‰ to +5.4 (Fig. 3). The running correlation coefficient between $\delta^{13}C$ and $\delta^{18}O$ shows a strong positive correlation for much of the timeseries, confirming as expected, that based on the water balance that the basin was closed and terminal throughout its existence (Li et al., 1997; Leng and Marshall, 2004). The running standard deviation of $\delta^{18}O$ from 2 Ma to 17 ka increases by a factor of 2 relative to the pre-2 Ma samples (Fig. S3). This is likely related to the onset of Northern Hemisphere glaciation and the intensification of glacial-interglacial cycles during the Pleistocene. There is also a gradual positive shift of about 10‰ in the oxygen isotopes from the base of the core to around 2 Ma. From 2 Ma to about 17 ka, there is a long-term negative trend in the oxygen isotopes of about 10‰.

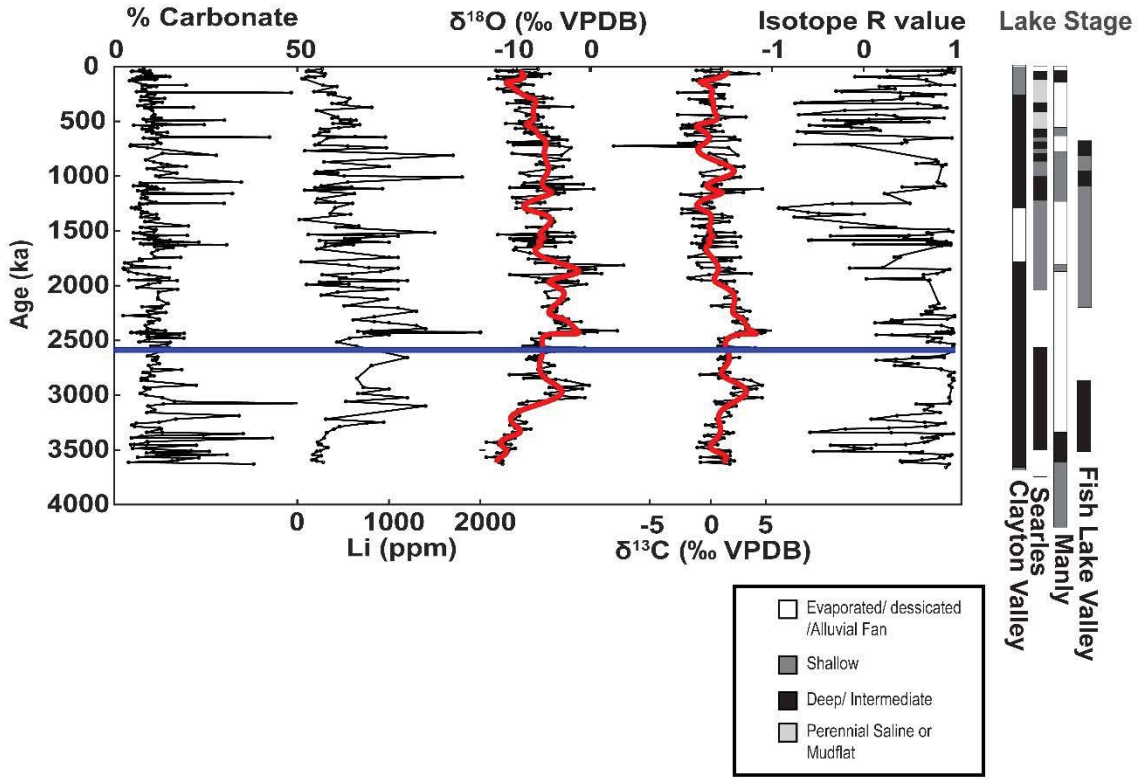

Figure 4. Timeseries from the Clayton Valley EXP2 core. From left to right: percent carbonate; bulk sediment lithium concentrations (ppm); carbonate $\delta^{18}O$ (‰, VPDB); carbonate $\delta^{13}C$ (‰, VPDB); running correlation coefficient between oxygen and carbon isotopes with a moving window of 10 data points; lake stage for Clayton Valley compared to neighboring valleys adapted after Knott et al. (2019). Solid red lines are a low pass filtered curve on the carbonate $\delta^{18}O$ and $\delta^{13}C$ records. Blue horizontal line marks the Pliocene-Pleistocene boundary.

There are a few hypotheses that may explain the long-term trend we observe from the mid-Pliocene to present. First, Quaternary uplift in the White Mountains and Sierra Nevada and subsequent blocking of winter moisture derived from the west of CV could have led to further depletion of source $\delta^{18}O$ via orographic effects (Lechler and Galewsky, 2013; Mix et al., 2019;

Hildreth et al., 2021). Second, changes in precipitation seasonality from summer precipitation to winter precipitation could drive source water $\delta^{18}O$ towards progressively depleted values. For example, this would entail the addition of moisture from a more northerly source during colder glacial periods rather than the central Pacific (Oster et al., 2020; discussed further below). Both changes in orographic rainout due to topographic changes or changes in seasonality would primarily influence the light endmembers in the observed oxygen isotope timeseries. Lastly, a gradual decrease in temperature through the Pleistocene and subsequent reduction in the effective evaporation could also lead to a more depleted lake water composition (i.e., less overall P-E). This effect would influence the declining average and the range in the observed oxygen isotope timeseries. As such, with existing data, because of the evaporative nature of lacustrine carbonate oxygen isotope records, we cannot necessarily rule out these scenarios. However, as described in the next section, data from adjacent basins with differential evaporation suggests that further orographic rainout can be ruled out (first scenario above associated with Quaternary uplift of the White Mountains and Sierra Nevada). Further, we can rule out an additional alternate scenario that changes in carbonate formation temperature (i.e., lake water temperature) influence our observations. Long term cooling would cause an increase not a decrease in the carbonate $\delta^{18}O$ values towards the present because of a larger fractionation factor between lake water and carbon at decreasing temperatures (Kim and O'Neil, 1997).

Comparison to Regional Records

There are multiple records of pluvial lakes in the region surrounding Clayton Valley ranging in age from the mid-Pliocene to the late Pleistocene which suggest a different regional moisture balance for this area of the Great Basin relative to today. The lake stages shown on

Figure 4, adapted from Knott et al. (2019), shows the interpreted lake stages for Clayton Valley (CV) and nearby lakes. Pluvial lakes in Death Valley (Lake Manly) (Lowenstein et al., 1999; Forester et al., 2005; Knott et al., 2018), to the south in Searles Valley (Smith et al., 1983; Jannik et al., 1991; Knott et al., 2018), and in Eureka Valley (Lake Andrei) began to form ~3.5–3.4 Ma in the late Pliocene during the cooler, wetter, glacial climate of MIS MG5 (Knott et al., 2019). The Death Valley lake persisted until ~3.30 Ma, while Searles lake persisted through the start of Northern Hemisphere glaciation until about 2.5 Ma. Lake Andrei was very short-lived, existing for only around 400,000 years (Knott et. al, 2019). Evidence from Fish Lake Valley suggests a lake existed from ca. 3.4 to 2.8 Ma (Reheis et al., 1993; Reheis et al., 2002; Knott et al., 2018). Lakes in these areas also existed intermittently during the Pleistocene. Pluvial lakes in Death Valley formed again ~1.98–1.78 Ma, 1.3–1.0 Ma, and ca. 0.6 Ma, while Searles Lake existed from about 2 Ma to the late Pleistocene. Fish Lake Valley sustained a lake in the middle Pleistocene ~2.2-0.7 Ma. A short-lived lake record also exists for Owens Valley (0.8 Ma to the late Pleistocene) (Smith et al., 1997).

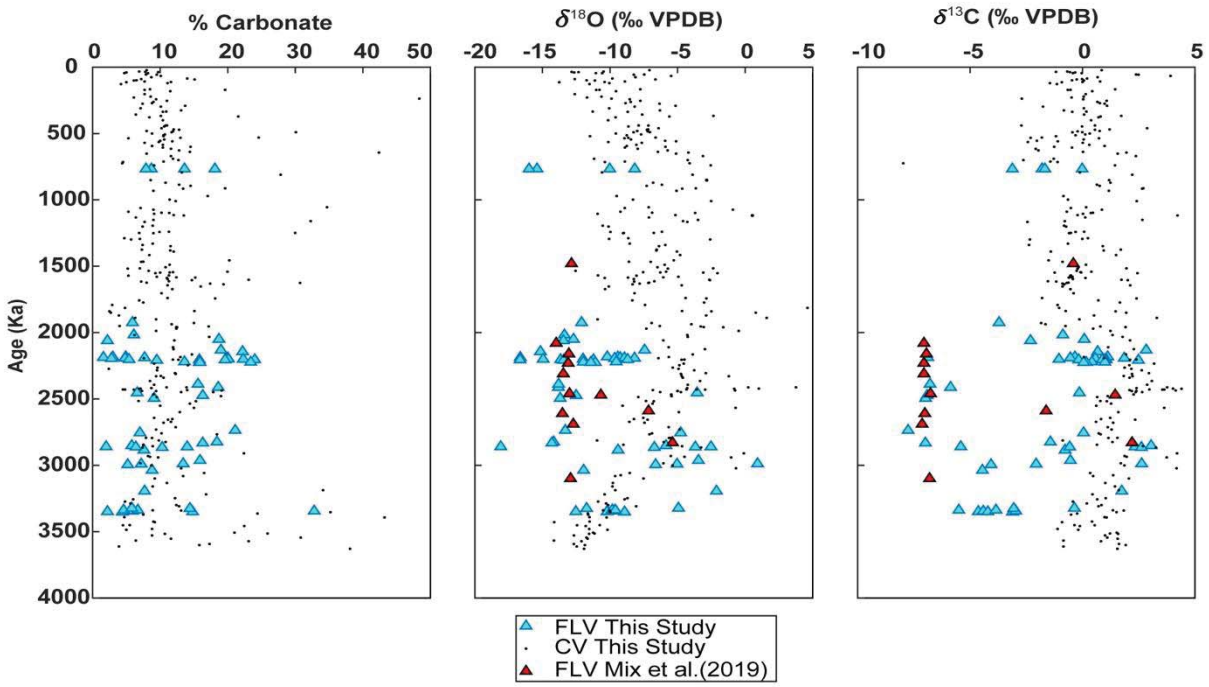

264

265 **Figure 5.** Stable isotopes of Clayton Valley carbonates compared to neighboring Fish Lake
266 Valley (FLV). FLV samples from this study (in blue) were collected in the summer of 2021. Red
267 samples are taken from Mix et al. (2019). Shown in black are values for Clayton Valley.

268

269 Stable isotope evidence from Fish Lake Valley (FLV), the adjacent valley to the west of
270 CV, and Clayton Valley lake stages suggest that the basins experienced asynchronous changes,
271 which could potentially be linked to uplift in the White Mountains and Sierra Nevada west of
272 FLV. Blocking of westerly moisture (Mix et al., 2019) could potentially have led to FLV drying
273 prior to CV (Reheis et al., 1993), which is why a shallow lake is observed for Clayton Valley
274 after Fish Lake Valley desiccated (by ~0.6 Ma). However, we would expect to see progressively
275 more depletion in oxygen isotopes as moisture moves eastward encountering subsequent
276 orographic rainout, into Fish Lake Valley, then into Clayton Valley. However, the oxygen
277 isotope record generated for Fish Lake Valley (*this study*; Mix et al., 2019) discredits this

278 potential scenario, as the lightest endmember $\delta^{18}O$ of Fish Lake Valley is more depleted than that
279 of Clayton Valley (Fig. 5).
280 Modern back trajectory analyses for Clayton Valley show the area receiving different
281 sources of water vapor depending on the season (Fig. 2). These different sources, which are
282 characterized by different isotopic compositions, could impact the source water composition of
283 the lake in Clayton Valley directly impacting the light $\delta^{18}O$ endmember of our record. Therefore,
284 we argue that the majority of the variance in the isotope record for Clayton Valley is controlled
285 by changes in seasonality and subsequent evaporative enrichment. Specifically, through the
286 Pliocene there is a shift to more summertime precipitation events likely related to an
287 enhancement of the convergent monsoonal circulation. Through the Pleistocene, we observe a
288 decrease in $\delta^{18}O$ values, which we attribute to the weakening of monsoonal circulation, and
289 strengthened southwesterly moisture delivery of wintertime precipitation.
290
291 *Hydroclimate controls on lithium enrichment*
292 The lithium concentrations in the clays are one to two orders of magnitude greater than
293 that of the average continental crust (Fig. 3), 35 ± 11 ppm (Teng et al., 2004). There is no
294 statistical correlation between lithium and sediment age, however there is a distinct positive
295 logarithmic correlation ($R^2 = 0.56$) between the paired measurements of lithium concentrations
296 and carbonate $\delta^{18}O$ (Fig. 6A). We generally observe higher $\delta^{18}O$ values in conjunction with
297 higher lithium concentrations.
298 Coffey et al. (2021) details the conceptual model for lithium brine development in basins
299 like Clayton Valley that we draw from here. Hydrothermal fluids rich in lithium interact with the
300 basin sediment. For example, results from Araoka et al. (2014) indicate that the lithium

concentrated in playas in Nevada was supplied mainly through high-temperature water–rock interaction associated with local hydrothermal activity and not directly by low-temperature weathering of surface materials. Basin sediments adsorb lithium, until groundwater liberates the adsorbed lithium into the shallow subsurface waters and outcropping water table. The lithium then becomes concentrated in the shallow subsurface brines through evapoconcentration. The findings of this study bear on the initial lithium enrichment of the basin sediments and link them to the hydroclimate evolution of the basin and lake system over the Pliocene-Pleistocene.

The covariance between the authigenic carbonate $\delta^{18}O$ in the lacustrine clays and the bulk lithium concentrations are related to the degree of evapoconcentration of the lake during authigenic clay and carbonate precipitation in the lake water (Fig. 6A). Variations in the past surface area to volume ratio of the lake could have an impact on the degree of effective evapoconcentration of the lake water. For example, early in the record (~3.6 to ~1.5 ka), as indicated by the CIA values and sedimentology (Figs. S2 and S3), P-E was relatively large, the lake was deep, and the surface area to volume ratio of the lake was likely smaller. This deep lake existed during this time, until the onset of halite deposition. The climate then transitions at ~1.5 ka to a lower P-E, the lake became smaller and frequently desiccated, due to the higher surface area to volume ratio of the shallower lake, there was highly effective evapoconcentration. These high concentration lithium values in the lake are driven by evaporation, which we propose is then incorporated into the structure and onto the surfaces of the authigenic clays precipitating in the lake water. Additionally, a survey of brine samples (Fig. 6B) demonstrates a similar logarithmic relationship between modern water $\delta^{18}O$ and brine lithium concentrations (*This Study;* Coffey et al., 2021) compared to the geologic EXP2 samples shown in Figure 5A.

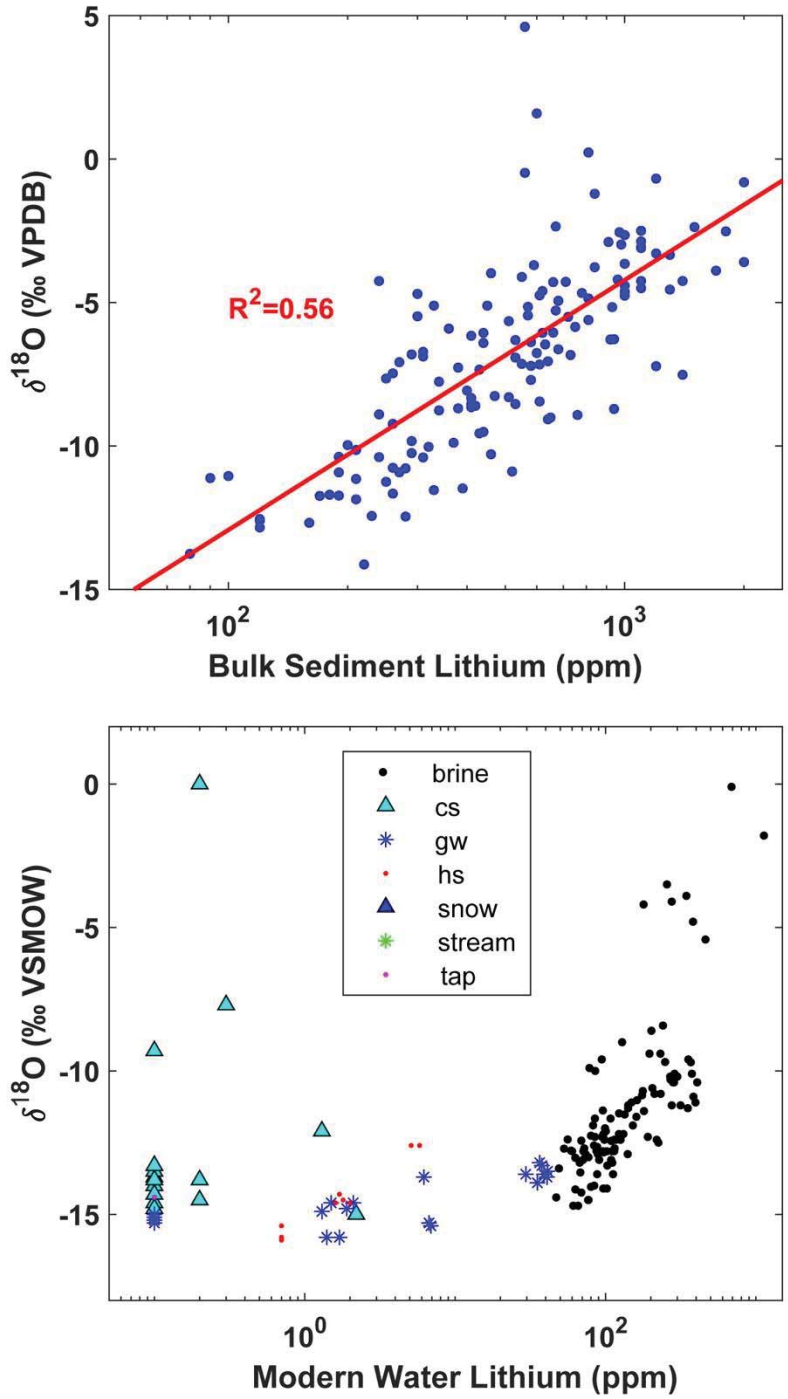

Figure 6. (A) Bulk sediment lithium concentrations (ppm) for EXP2 samples paired with carbonate oxygen isotope values (VPDB). The red line is a logarithmic fit with an R^2 value of 0.56. (B) Lithium (ppm) and oxygen isotope values (VSMOW) of natural modern water samples.

There is a question of whether the lithium became incorporated into the clays post deposition due to hydrothermal interactions, or if the clays incorporated the lithium during initial genesis in the lake water (cf. Coffey et al., 2021). The covariance between $\delta^{18}O$ and lithium concentrations (Fig. 6) and the thin sections show no evidence for post-depositional alteration (Fig. S4), suggesting that the lithium became incorporated in the clays at the time of formation, and not post-depositionally. Future work analyzing the oxygen, hydrogen and lithium isotopes of clay fractions from EXP2 may demonstrate this link more concretely.

CONCLUSION

Our lacustrine carbonate isotope record for Clayton Valley, NV reveals a rich continuous history of hydroclimate spanning the last ~3.6 Myrs. We argue that while the lake sustains high overall isotope values due to evaporative enrichment, million-year scale variations are driven by changes in the seasonality of precipitation being sourced to the basin as well as changes in P-E. Specifically, we argue that the mid-Pliocene to early Pleistocene saw enhanced convergent monsoonal circulation, and through the Pleistocene, strengthened southwesterly moisture delivery could have resulted in greater wintertime precipitation. We find a covariance between carbonate oxygen isotopes and paired bulk lithium concentrations, which we attribute to the effects of evapoconcentration prior to authigenic clay precipitation in the lake water. This finding suggests that climate may play a key role in the concentration of lithium in authigenic lacustrine clays.

ACKNOWLEDGEMENTS

This work was partially supported by NSF/GSA Graduate Student Geoscience Grant # 13087-21 to CAG, which is funded by NSF Award # 1949901, and funding from the Miller Institute at UC Berkeley to DEI. TB was supported by NSF P2C2 Grant OCE-1903148. DEI and CG were partially supported by P2C2 Grant AGS-2102901. We greatly appreciate the Albermarle Corporation for providing access to CV drill cores. We would like to thank Steven Clemens for assistance with the carbonate stable isotope measurements; Hari Mix and Michele Bezanson for help with fieldwork; and Sylvia Dee and Jim Russell for lake discussions and assistance with HYSPLIT analyses.

REFERENCES

Annan, J. D., & Hargreaves, J. C.,2013, A new global reconstruction of temperature changes at the Last Glacial Maximum: *Climate of the Past*, v. *9*, p. 367-376.

Araoka, D., Kawahata, H., Takagi, T., Watanabe, Y., Nishimura, K., & Nishio, Y.,2014, Lithium and strontium isotopic systematics in playas in Nevada, USA: constraints on the origin of lithium: *Mineralium Deposita*, v. *49*, p. 371-379.

Bhattacharya, T., Tierney, J. E., & DiNezio, P.,2017, Glacial reduction of the North American Monsoon via surface cooling and atmospheric ventilation: *Geophysical Research Letters*, v. *44*, p. 5113-5122.

Bradley, D. C., Munk, L., Jochens, H., Hynek, S., & Labay, K.,2013, *A preliminary deposit model for lithium brines*: US Department of the Interior, US Geological Survey.

Brooks, L. E., Masbruch, M. D., Sweetkind, D. S., & Buto, S. G., 2014, Steady-state numerical groundwater flow model of the Great Basin carbonate and alluvial aquifer system: *US Geological Survey Scientific Investigation Report*, 124.

374 Burke, K. D., Williams, J. W., Chandler, M. A., Haywood, A. M., Lunt, D. J., & Otto-Bliesner,
375 B. L., 2018, Pliocene and Eocene provide best analogs for near-future climates:
376 *Proceedings of the National Academy of Sciences*, v. *115*, p. 13288-13293.
377 Burls, N. J., & Fedorov, A. V.,2017, Wetter subtropics in a warmer world: Contrasting past and
378 future hydrological cycles: *Proceedings of the National Academy of Sciences*, v. *114*, p.
379 12888-12893.
380 Burrus, J. B., 2013, Structural and stratigraphic evolution of the Weepah Hills Area, NV:
381 transition from basin-and-range extension to Miocene core complex formation[Master's
382 Thesis]: University of Texas at Austin.
383 Carroll, A. R., & Bohacs, K. M.,1999, Stratigraphic classification of ancient lakes: Balancing
384 tectonic and climatic controls: *Geology*, v. *27*, p. 99-102.
385 Castor, S. B., & Henry, C. D., 2020, Lithium-rich claystone in the McDermitt Caldera, Nevada,
386 USA: Geologic, mineralogical, and geochemical characteristics and possible origin:
387 *Minerals*, v. *10*, p. 68.
388 Clark, P. U., Dyke, A. S., Shakun, J. D., Carlson, A. E., Clark, J., Wohlfarth, B., Mitrovica, J.X.,
389 Hostetler, S. W., McCabe, A. M.,2009, The last glacial maximum: *Science*, v. *325*, p.
390 710-714.
391 Coffey, D. M., Munk, L. A., Ibarra, D. E., Butler, K. L., Boutt, D. F., & Jenckes, J., 2021,
392 Lithium Storage and Release from Lacustrine Sediments: Implications for Lithium
393 Enrichment and Sustainability in Continental Brines: *Geochemistry, Geophysics,*
394 *Geosystems*, v. 22, p. e2021GC009916.
395 Davis, J. R., Friedman, I., & Gleason, J. D., 1986, Origin of the lithium-rich brine, Clayton
396 Valley, Nevada: *US Geological Survey Bulletin*, v. *1622*, p. 131-138.

Dowsett, H. J., & Caballero Gill, R. P., 2010, Pliocene climate: *Stratigraphy*, v. *7*, p. 106-110.

Forester, R. M., Lowenstein, T. K., & Spencer, R. J., 2005, An ostracode based paleolimnologic and paleohydrologic history of Death Valley: 200 to 0 ka: *Geological Society of America Bulletin*, v. *117*, p. 1379-1386.

Fu, M., Cane, M. A., Molnar, P., & Tziperman, E., 2022, Warmer Pliocene upwelling site SST leads to wetter subtropical coastal areas: a positive feedback on SST: *Paleoceanography and Paleoclimatology*, v. 37, p. e2021PA004357.

Godsey, H. S., Oviatt, C. G., Miller, D. M., & Chan, M. A., 2011, Stratigraphy and chronology of offshore to nearshore deposits associated with the Provo shoreline, Pleistocene Lake Bonneville, Utah: *Palaeogeography, Palaeoclimatology, Palaeoecology*, v. *310*, p. 442-450.

A.M. Haywood, J.C. Tindall, H.J. Dowsett, A.M. Dolan, K.M. Foley, S.J. Hunter, D.J. Hill, W.L. Chan, A. Abe-Ouchi, C. Stepanek, G. Lohmann, D. Chandan, W.R. Peltier, N. Tan, C. Contoux, G. Ramstein, X. Li, Z. Zhang, C. Guo, K.H. Nisancioglu, Q. Zhang, Q. Li, Y. Kamae, M.A. Chandler, L.E. Sohl, B.L. Otto-Bliesner, R. Feng, E.C. Brady, A.S. von der Heydt, M.L.J. Baatsen, D.J. Lunt, 2020, The Pliocene Model Intercomparison Project Phase 2: large-scale climate features and climate sensitivity: *Climate of the Past*, v. *16*, p. 2095-2123.

Hildreth, W., Fierstein, J., Phillips, F. M., & Calvert, A., 2021, Trachyandesite of Kennedy Table, its vent complex, and post− 9.3 Ma uplift of the central Sierra Nevada: *GSA Bulletin*.

Ibarra, D. E., Oster, J. L., Winnick, M. J., Caves Rugenstein, J. K., Byrne, M. P., & Chamberlain, C. P., 2018, Warm and cold wet states in the western United States during the Pliocene–Pleistocene. *Geology*, v. *46*, p. 355-358.

Ibarra, D. E., Egger, A. E., Weaver, K. L., Harris, C. R., & Maher, K., 2014, Rise and fall of late Pleistocene pluvial lakes in response to reduced evaporation and precipitation: Evidence from Lake Surprise, California: *GSA Bulletin*, v. 126, p. 1387-1415.

Ingersoll, R. V., 2019, Subduction-Related Sedimentary Basins of the US Cordillera, *in* The Sedimentary Basins of the United States and Canada, Elsevier, p. 477-510.

Jannik, N. O., Phillips, F. M., Smith, G. I., & Elmore, D., 1991, A 36Cl chronology of lacustrine sedimentation in the Pleistocene Owens River system: *GSA Bulletin*, v. *103*, p. 1146-1159.

Kim, S. T., & O'Neil, J. R., 1997, Equilibrium and nonequilibrium oxygen isotope effects in synthetic carbonates: *Geochimica et cosmochimica acta*, v. *61*, p. 3461-3475.

Knott, J. R., Machette, M. N., Wan, E., Klinger, R. E., Liddicoat, J. C., Sarna-Wojcicki, A. M., Fleck, R. J., Deino, A. L., Geissman, J. W., Slate J. L., Wahl D. B., Wernicke, B. P., Wells, S. G., Tinsley III, Hathaway, J. C., Weamer, V. M., 2018, Late Neogene–Quaternary tephrochronology, stratigraphy, and paleoclimate of Death Valley, California, USA: *GSA Bulletin*, v. *130*, p. 1231-1255.

Knott, J. R., Wan, E., Deino, A. L., Casteel, M., Reheis, M. C., Phillips, F. M., Walkup, L., McCarty, K., Manoukian, D. N., Nunez, E., 2019, Lake Andrei: A pliocene pluvial lake in Eureka Valley, eastern California: *From Saline to Freshwater: The Diversity of Western Lakes in Space and Time, S. Starratt and MR Rosen, Eds*, *536*, 125-142.

Kurth, G., Phillips, F. M., Reheis, M. C., Redwine, J. L., & Paces, J. B., 2011, Cosmogenic nuclide and uranium-series dating of old, high shorelines in the western Great Basin, USA: *GSA Bulletin*, v. *123*, p. 744-768.

Lee, J.-Y., J. Marotzke, G. Bala, L. Cao, S. Corti, J.P. Dunne, F. Engelbrecht, E. Fischer, J.C. Fyfe, C. Jones, A. Maycock, J. Mutemi, O. Ndiaye, S. Panickal, and T. Zhou, 2021, Future Global Climate: Scenario-Based Projections and Near-Term Information. In Climate Change 2021: The Physical Science Basis. Contribution of Working Group I to the Sixth Assessment Report of the Intergovernmental Panel on Climate Change [Masson-Delmotte, V., P. Zhai, A. Pirani, S.L. Connors, C. Péan, S. Berger, N. Caud, Y. Chen, L. Goldfarb, M.I. Gomis, M. Huang, K. Leitzell, E. Lonnoy, J.B.R. Matthews, T.K. Maycock, T. Waterfield, O. Yelekçi, R. Yu, and B. Zhou (eds.)]. Cambridge University Press. In Press.

Leng, M. J., & Marshall, J. D., 2004, Palaeoclimate interpretation of stable isotope data from lake sediment archives: *Quaternary Science Reviews*, v. *23*, p. 811-831.

Li, H. C., & Ku, T. L., 1997, δ13C–δ18C covariance as a paleohydrological indicator for closed-basin lakes: *Palaeogeography, Palaeoclimatology, Palaeoecology*, v. *133*, p. 69-80.

Lora, J. M., & Ibarra, D. E., 2019, The North American hydrologic cycle through the last deglaciation: *Quaternary Science Reviews*, v. *226*, p. 105991.

Lowenstein, T. K., Li, J., Brown, C., Roberts, S. M., Ku, T. L., Luo, S., & Yang, W., 1999, 200 ky paleoclimate record from Death Valley salt core: *Geology*, v. *27*, p. 3-6.

Manthiram, A., 2017, An outlook on lithium ion battery technology. *ACS central science*, v. 3(10), p. 1063-1069.

462 Matsubara, Y., and Howard, A.D., 2009, A spatially explicit model of runoff, evaporation, and
463 lake extent: Application to modern and late Pleistocene lakes in the Great Basin region,
464 western United States: *Water Resources Research*, v. 45.
465 Means, J.D., 2013, GPS precipitable water as a diagnostic of the North American monsoon in
466 California and Nevada: *Journal of Climate*, v. *26*, p. 1432-1444.
467 Mifflin M.D. Wheat M.M., 1979, Pluvial Lakes and Estimated Pluvial Climates of Nevada:
468 Nevada Bureau of Mines and Geology Bulletin, v. 94, 57 p.
469 Mix, H. T., Rugenstein, J. K. C., Reilly, S. P., Ritch, A. J., Winnick, M. J., Kukla, T., &
470 Chamberlain, C. P., 2019, Atmospheric flow deflection in the late Cenozoic Sierra
471 Nevada: *Earth and Planetary Science Letters*, v. *518*, p. 76-85.
472 Munk, L., & Chamberlain, C. P., 2011, Final Technical Report: G10AP00056-Lithium Brine
473 Resources: A Predictive Exploration Model. *Research supported by the US Geological*
474 *Survey (USGS), Department of the Interior, under USGS award*, (G10AP00056).
475 Munk, L., Jennings, M., Bradley, D., Hynek, S., Godfrey, L., & Jochens, H. (2011, September).
476 Geochemistry of lithium-rich brines in Clayton Valley, Nevada, USA. In *Proceedings of*
477 *the 11th SGA Biennial Meeting, Antofagasta, Chile* (pp. 26-29).
478 Munk, L. A., Hynek, S. A., Bradley, D., Boutt, D., Labay, K., & Jochens, H., 2016, Lithum
479 brines: A global perspective: *Reviews in Economic Geology*, v. 18, p. 339-365.
480 Munroe, J. S., & Laabs, B. J., 2013, Latest Pleistocene history of pluvial Lake Franklin,
481 northeastern Nevada, USA: *GSA Bulletin*, v. *125*, p. 322-342.
482 Oldow, J. S., Elias, E. A., Ferranti, L., McClelland, W. C., McIntosh, W. C., & Cashman, P. H.,
483 2009, Late Miocene to Pliocene synextensional deposition in fault-bounded basins within
484 the upper plate of the western Silver Peak–Lone Mountain extensional complex, west-

485 central Nevada: *Late Cenozoic Structure and Evolution of the Great Basin–Sierra*
486 *Nevada Transition: Geological Society of America Special Paper*, *447*, 275-312.
487 Orme, A. R., 2008, Pleistocene pluvial lakes of the American West: a short history of research:
488 *Geological Society, London, Special Publications*, v. *301*, p. 51-78.
489 Oster, J. L., & Ibarra, D. E., 2018, Glacial hydroclimate of western North America: insights from
490 proxy-model comparison and implications for Lake Bonneville, *Utah Geological Survey*
491 *Miscellaneous Publications,* v. 170, p. 8.
492 Oster, J. L., Weisman, I. E., & Sharp, W. D., 2020, Multi-proxy stalagmite records from northern
493 California reveal dynamic patterns of regional hydroclimate over the last glacial cycle:
494 *Quaternary Science Reviews*, v. *241*, p. 106411.
495 Pound, M. J., Tindall, J., Pickering, S. J., Haywood, A. M., Dowsett, H. J., & Salzmann, U.,
496 2014, Late Pliocene lakes and soils: a global data set for the analysis of climate feedbacks
497 in a warmer world: *Climate of the Past*, v. *10*, p. 167-180.
498 Ravelo, A. C., Andreasen, D. H., Lyle, M., Olivarez Lyle, A., & Wara, M. W., 2004, Regional
499 climate shifts caused by gradual global cooling in the Pliocene epoch: *Nature*, v. *429*, p.
500 263-267.
501 Ray, A. J., Garfin, G. M., Wilder, M., Vásquez-León, M., Lenart, M., & Comrie, A. C., 2007,
502 Applications of monsoon research: Opportunities to inform decision making and reduce
503 regional vulnerability: *Journal of Climate*, v. *20*, p. 1608-1627.
504 Reheis, M. C., Adams, K. D., Oviatt, C. G., & Bacon, S. N., 2014, Pluvial lakes in the Great
505 Basin of the western United States—a view from the outcrop: *Quaternary Science*
506 *Reviews*, v. *97*, p. 33-57.

507 Reheis, M.,1999, Highest pluvial-lake shorelines and Pleistocene climate of the western Great
508 Basin: *Quaternary research*, v. *52*, p. 196-205.
509 Reheis M.C.,1999a, Extent of Pleistocene Lakes in the Western Great Basin: U.S. Geological
510 Survey Miscellaneous Field Studies Map MF-2323, scale 1:800, 000, 1 sheet.
511 Reheis, M. C., Slate, J. L., Sarna-Wojcicki, A. M., & Meyer, C. E.,1993, A late Pliocene to
512 middle Pleistocene pluvial lake in Fish Lake Valley, Nevada and California: *Geological*
513 *Society of America Bulletin*, v. *105*, p. 953-967.
514 Reheis, M. C., A. M. Sarna-Wojcicki, R. L. Reynolds, C. A. Repenning, and M. D. Mifflen,
515 2002, Pliocene to middle Pleistocene lakes in the western Great Basin: Ages and
516 connections, in Great Basin Aquatic Systems History, edited by R. Hershler, D. Currey,
517 and D. Madsen, Smithson. Contrib. Earth Sci., v. 33, p. 53–108.
518 Rush, F. E.,1968, *Water-resources Appraisal of Clayton Valley-Stonewall Flat Area, Nevada*
519 *and California*. State of Nevada, Department of Conservation and Natural Resources.
520 Salzmann, U., Williams, M., Haywood, A. M., Johnson, A. L., Kender, S., & Zalasiewicz, J.,
521 2011, Climate and environment of a Pliocene warm world: *Palaeogeography,*
522 *Palaeoclimatology, Palaeoecology*, v. *309*, p. 1-8.
523 Santi, L. M., Arnold, A. J., Ibarra, D. E., Whicker, C. A., Mering, J. A., Lomarda, R. B., Lora, J.
524 M., Tripati, A., 2020, Clumped isotope constraints on changes in latest Pleistocene
525 hydroclimate in the northwestern Great Basin: Lake Surprise, California: *GSA Bulletin*, v.
526 *132*, p. 2669-2683.
527 Smith, G. I.,1983, Core KM-3, a surface-to-bedrock record of late Cenozoic sedimentation in
528 Searles Valley, California.

529 Smith, G.I., Bishchoff, J.L., and Bradbury, J.P., 1997, Synthesis of the paleoclimatic record from
530 Owens Lake core OL-92, in Smith, G.I., and Bishchoff, J.L.,eds., An 800,000-Year
531 Paleoclimatic Record from Core OL-92: Geological Society of America Special Paper
532 317,p. 143–160.
533 Stein, A. F., Draxler, R. R., Rolph, G. D., Stunder, B. J., Cohen, M. D., & Ngan, F., 2015,
534 NOAA's HYSPLIT atmospheric transport and dispersion modeling system: *Bulletin of*
535 *the American Meteorological Society*, v. *96*, p. 2059-2077.
536 Sweetkind, D. S., Masbrunch, M. D., Heilweil, V. M., & Buto, S. G. (2010). Chapter C:
537 Groundwater flow. In V. M. Heilweil, & L. E. Brooks (Eds.), Conceptual model of the
538 Great Basin carbonate and alluvial aquifer system (p. 191). U.S. Geological Survey
539 Scientific Investigations Report 2010-5193.
540 Teng, F. Z., McDonough, W. F., Rudnick, R. L., Dalpé, C., Tomascak, P. B., Chappell, B. W., &
541 Gao, S., 2004, Lithium isotopic composition and concentration of the upper continental
542 crust: *Geochimica et Cosmochimica Acta*, v. *68*, p. 4167-4178.
543 Underdown, C. G., Boutt, D. F., Hynek, S. A., & Munk, L. A., 2017, Evaluating Hydrologic
544 Transience in Watershed Delineation, Numerical Modeling and Solute Transport in the
545 Great Basin. Clayton Valley, Nevada: *AGU Fall Meeting Abstracts,* v. 2017, p. H53O-
546 08).
547 Warner, M. S., 2018, Introduction to PySPLIT: A Python toolkit for NOAA ARL's HYSPLIT
548 model: *Computing in Science & Engineering*, v. *20*, p. 47-62.
549 Welker, J. M.,2012, ENSO effects on δ18O, δ2H and d-excess values in precipitation across the
550 US using a high-density, long-term network (USNIP): *Rapid Communications in Mass*
551 *Spectrometry*, v. *26*, p. 1893-1898.

552

SUPPLEMENTARY MATERIALS

for

Paleoclimate controls on lithium enrichment in Great Basin Pliocene-Pleistocene lacustrine clays

Catherine A. Gagnon[1,2,†], Kristina L. Butler[3], Elizabeth Gaviria[1,4], Alexa Terrazas[5], Annabelle Gao[1], Tripti Bhattacharya[6], David F. Boutt[7], Lee Ann Munk[8], Daniel E. Ibarra[1,2]

[1]Department of Earth, Environmental and Planetary Science, Brown University, Providence, RI 02912, USA

[2]Institute at Brown for Environment and Society, Brown University, Providence, RI 02912, USA

[3]Department of Geological Sciences, Jackson School of Geosciences, University of Texas at Austin, Austin, TX 78712, USA

[4]Department of Earth, Environmental and Planetary Sciences, Rice University, Houston, TX 77005, USA

[5]Department of Ocean and Atmospheric Sciences, University of California, Los Angeles, CA, 90095, USA

[6]Department of Earth Sciences, Syracuse University, Syracuse, NY 12344, USA

[7]Department of Geosciences, University of Massachusetts-Amherst, Amherst, MA 01003, USA

[8]Department of Geological Sciences, University of Alaska Anchorage, Anchorage, AK 99508, USA

† Corresponding author: catherine_gagnon@brown.edu

The following is included in this file:

Figure S1. Zircon U-Pb age

Figure S2. CIA ternary diagram

Figure S3. Timeseries of all datasets from EXP2

Figures S4. Thin sections

The following is included in an attached Excel File:

Table S1. EXP2 age constraints

Table S2. EXP2 samples and data table

Table S3. Zircon U-Pb data

Table S4. 40Ar/39Ar data

Table S5. Fish Lake Valley age constraints

Table S6. Fish Lake Valley samples and data table

Table S7. Modern water samples

Precipitation Back-Trajectory Analyses

Back-trajectories were generated using the desktop version of the Hybrid Single-Particle Lagrangian Integrated Trajectory (HYSPLIT) model and the North American Regional Reanalysis (NARR) as the HYSPLIT meteorological input. We tracked air parcels backwards for 72 hours every 24 hours at 1500 meters above ground level to gauge the precipitation sources of each of the study sites. Daily 72 hour back-trajectories began at the end of the day and were generated for every day between 1979-2019, which covers the extent of the NARR climate record.

In order to filter trajectories by precipitation events, we used weather station data in the Global Historical Climatology Network-Daily (GHCN-D) database, keeping both geographical location and elevation as close as possible. The station record from Silverpeak NV (within Clayton Valley) records historic snow and rain events throughout 1979-2019, both of which are considered in our precipitation analyses. For each site, trajectories were matched with the corresponding day in the meteorological record and filtered based on whether there was any rain or snow for that day. Days that were missing both a rain and snow record were not included in the analyses. The resulting precipitation trajectories were then filtered by summer (April-September) and winter (October-March) half year months.

Once the precipitation-carrying trajectories were filtered, a cluster analysis was completed for each site's summer, and winter trajectories using HYSPLIT's built-in clustering program. The number of clusters in each analysis was determined by the change in Total Spatial Variance (TSV) curve generated as clusters were combined. The point at which the fewest number of clusters had a change in TSV less than about 15% was selected for the analysis. The trajectories in each cluster were then averaged and plotted on a map with a topographic overlay. Finally, we weighted the cluster means by total precipitation delivered. The thickness of the lines on Figure 1 are scaled to this weighting.

A similar set of HYSPLIT analyses (without clustering) was conducted for weekly precipitation samples from the NV00 site at Red Rock Canyon (36.13483 ºN, -115.422 ºW, 1,137 m) from the USNIP network (Welker, 2012), the closest site to CV. Shown on Figure 2A are daily trajectories for all days with precipitation colored by the oxygen isotope value of the weekly aggregated rainfall. This station contains data spanning May 1989 to December 1994, with 29 total weeks of isotope data.

Dating Methods, Age Model and Sample Age Assignment

In previous work Coffey et al. (2021) dated six ashes from the EXP cores using $^{40}Ar/^{39}Ar$ methods on sanidine. In this work we presented two additional $^{40}Ar/^{39}Ar$ age and one zircon U-Pb ages to refine the age model for EXP2.

For the new $^{40}Ar/^{39}Ar$ ages at 336.35 m and 774.8 m, sanidine and plagioclase (respectively) were isolated from the tephras via magnetic and density sorting techniques, and their composition was verified using a variable pressure scanning electron microscope. Separates were wrapped in aluminum foil, placed in 2.5 cm aluminum disks, and irradiated along with the 1.1864 Ma Alder Creek sanidine standard (Jicha et al., 2016) at the Oregon State University TRIGA reactor in the Cadmium-Lined In-Core Irradiation Tube (CLICIT). Single crystal fusion experiments were performed with a 50 W CO_2 laser in the WiscAr laboratory at the University of Wisconsin-Madison. Gas was analyzed using a Noblesse multi-collector mass spectrometer using the procedures in Jicha et al. (2016). Weighted mean ages are calculated using the decay constants of Min et al. (2000), and are reported with analytical uncertainties at the 95% confidence level. Atmospheric argon value used is that of Lee et al. (2006).

One volcanic ash sample (EXP2_3277) was collected from Albemarle Corporation EXP2 drill core for zircon U-Pb crystallization age at 998.8 m. Zircon grains were isolated by traditional physical and chemical mineral separation methods, including crushing, grinding, and hydraulic, heavy-liquid, and magnetic separation. Zircon grains were then poured onto double-sided tape on epoxy resin mounts and 33 inclusion-free zircons were selected for U-Pb analysis by laser ablation–inductively coupled plasma–mass spectrometry (LA-ICP-MS) at the University of Texas at Austin. Mounts were transferred to a large-volume Helex sample cell and analyzed by a magnetic sector, single collector Element2 HR-ICP-MS with an attached PhotonMachine

Analyte G.2 Excimer Laser ablation system. Data reduction was performed in the Iolite software (Paton et al., 2011). A weighted mean average age (6.134 ± 0.095 Ma) was calculated from a unimodal population of 16 zircon ages, with an MSWD of 0.78. Ages with discordance >30% were excluded from the age calculation. Weight Mean Average plot and Whetherill Concordia were constructed using IsoplotR (Fig. S1; Vermeesch, 2018). See Table S3 for zircon U-Pb analytical results.

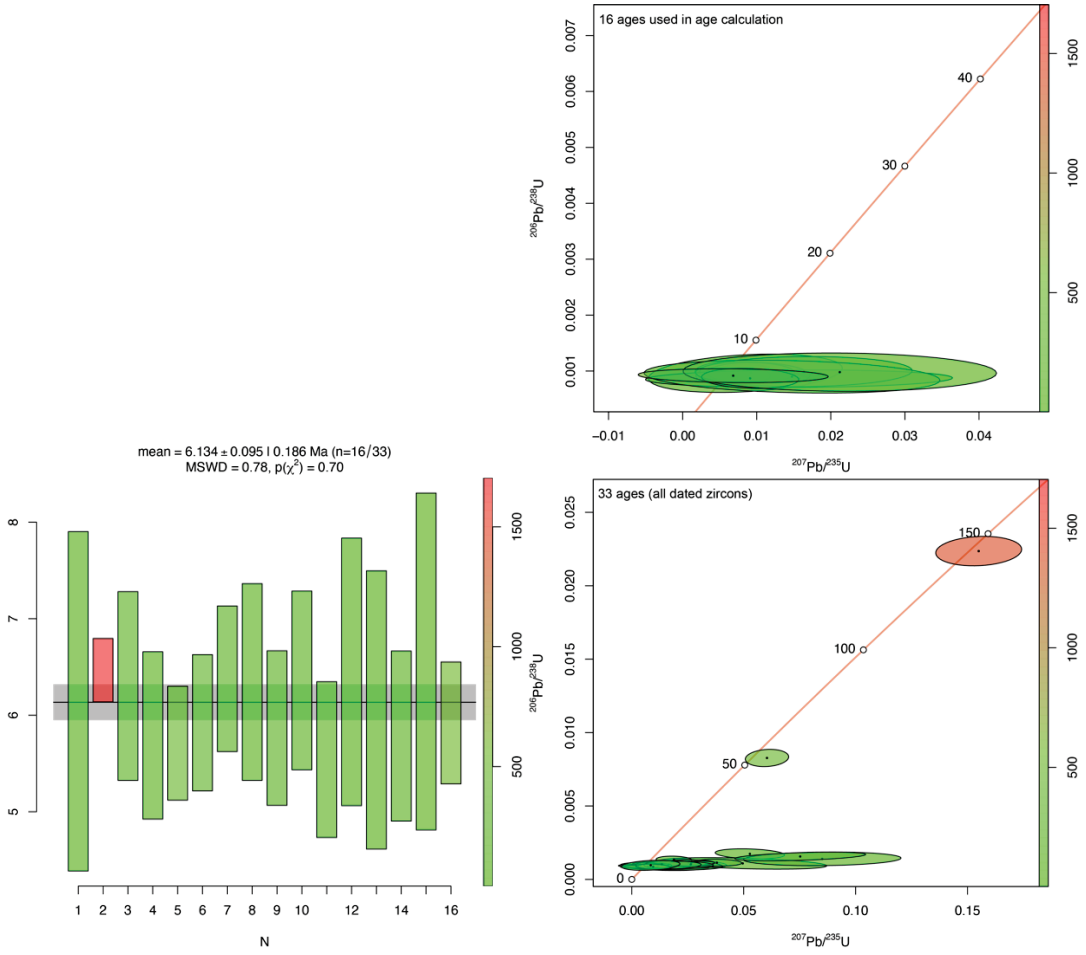

Figure S1. Weighted Mean Average age plot (left) showing 16/33 zircon ages used to calculate volcanic ash age for sample EXP2_3277, and Whetherill Concordia plots (right) showing (top) 16/33 ages used to calculate volcanic ash age and (bottom) all 33 zircon ages for sample

EXP2_3277. Color scale bars on all plots show approximate U ppm. Plots were made in IsoplotR (Vermeesch, 2018).

In the following we describe our age model constraints from top to bottom. First, we assumed that the top of the core to be Holocene (5±5 ka). The first age used in our core comes from a relatively thick ash at 184.4 m which we have correlated in other regional cores to be the Lava Creek B Yellowstone eruption. The main ash aquifer in Clayton Valley is the Bishop Tuff (Long Valley Caldera), this thick ash unit appears in all 5 Clayton Valley cores (Coffey et al., 2021) at only slightly offset depths. This ash was verified in EXP1 by Coffey et al. (2021) to be the Bishop Tuff. The next four dates used were constrained with $^{40}Ar/^{39}Ar$, including our new ages of 1,145.7±10.8 ka (at 336.35 m), and 2,476 ± 68 ka (at 774.8 m), while the last age was determined by zircon U-Pb of the basal lithic tuff unit (6,134 ± 95 ka). Because of an apparent change (increase) in sedimentation rate at the base of the core, the relatively few number of ages, and the otherwise linear nature of our age-depth relationship, we construct a simple age model using a Monte-Carlo based age-depth model using and assigned probable ages to all samples. The three probable scenarios at the base of the core shown in Figure 2 include: 1) extrapolation of the above sedimentation rate, 2) a maximum sedimentation rate assuming no hiatuses, and 3) an average of 1) and 2). For the purposes of plotting our measurements vs. age in Figure 4 and Figure S3 we use scenario three. However, we note that the interpretation of our dataset in this paper is not influenced by these assumptions.

126 ***FLV Outcrop Samples and Age Model***

127 The FLV samples used to generate the carbonate stable isotope values in this study were
128 outcrop samples collected in the summer 2021 field season. We visited the southeast playa and
129 rimrock sections (Reheis et al., 1991, their Figures 2 & 4) as well as the northeast 179-EP section
130 (Reheis et al., 1993; their Figure 7). We attributed depths/heights to the outcrop samples relative
131 to boundaries of units described by Reheis (1991, 1993). We then used a combination of
132 previously dated ashes (Knott et al., 2018; 2019) and previously correlated magnetostratigraphy
133 (Sarna-Wojcicki et al., 2005; their figure 15) following Mix et al. (2019) (Tables S5 and S6).

134

135 ***Carbonate Stable Isotope Analyses***

136 The samples that were analyzed at Brown University were first dried overnight at 60 ºC,
137 then homogenized via mortar and pestle. Of the sample, 500 μg were weighed out and reacted
138 with 70 degree C phosphoric acid using a Thermo Finnigan Kiel III or Kiel IV carbonate device.
139 This measured weight is based on a typical 10% sample carbonate content and a required 50
140 micrograms of $CaCO_3$ for the desired range of measurement voltage (3 to 6 V). The evolved CO_2
141 was measured on either a Thermo Finnigan MAT 252 gas-ratio mass spectrometer or Thermo
142 Finnigan MAT 253+ (Table 1, Table S1). External precision (1σ) of oxygen and carbon isotope
143 data is <0.1‰, based upon repeated measurements of two internal laboratory standards,
144 BYM63150 and Carrara63150, calibrated against NBS 18, NBS 19, and IAEA 603.

145 The samples that were analyzed at Stanford University in 2018 were homogenized via
146 mortar and pestle. Stable carbon and oxygen isotope values of carbonates were obtained at the
147 Stable Isotope Biogeochemistry Laboratory, Stanford University, using a Thermo Finnigan
148 Gasbench and measured on a Finnigan MAT Delta+ XL mass spectrometer using a Thermo

Finnigan ConFlo III unit. Approximately 300 μg of sample powder was weighed into sealed vials that were flushed with He gas and reacted with ca. 0.25 ml of phosphoric acid (H3PO4) for 1 hour at 72°C. External precision (1σ) of oxygen and carbon isotope data is <0.1‰, based upon repeated measurements of two internal laboratory standards calibrated against NBS 18, NBS 19, and LSVEC. $\delta^{13}C$ and $\delta^{18}O$ values are reported relative to VPDB for datasets from both laboratories.

Whole Rock Elemental Analyses and Lithium Concentrations

As in Coffey et al. (2021) whole rock samples were analyzed by SGS Environmental Services for whole rock geochemistry by X-ray fluorescence and Inductively Coupled Plasma Emission Spectrometry.

Briefly, approximately 1 gram of crushed and pulverized samples were formed into a homogenous glass disk by fusion with a lithium tetraborate/lithium metaborate mixture and then analyzed by wavelength dispersion XRF (WD-XRF). All reporting limits are less than or equal to 0.01%. Calibration checks are performed daily. SGS methods conform to the ISO/IEC/17025. Lithium concentrations on solid samples were performed by ICP-OES by SGS. A 0.1 gram sample of crushed and pulverized sample was fused using Na_2O_2 and digested in HCl, and Li concentrations analyzed on an Agilent ICP-OES.

Weathering Indices

The results of the CIA calculations are summarized in Figure S2 and shown in the timeseries in Figure S3. There does not appear to be a distinction between the lithologies in terms of the CIA values, with most plotting close to the Ca/Na and Al endmembers. There are,

however, distinct shifts in the CIA value time series (Figure S3). From the base of the core, the CIA values stay below 40 until they reach the top of the halite beds where they then increase their weathered CIA value to ~60. The weathering indices stay high until the base of the thick ash at ~750 ka where they drop to below 40. From the base of the ash to the top of the core the CIA values then increase gradually. We also plot Si/Al on Figure S3, which shows similar trends.

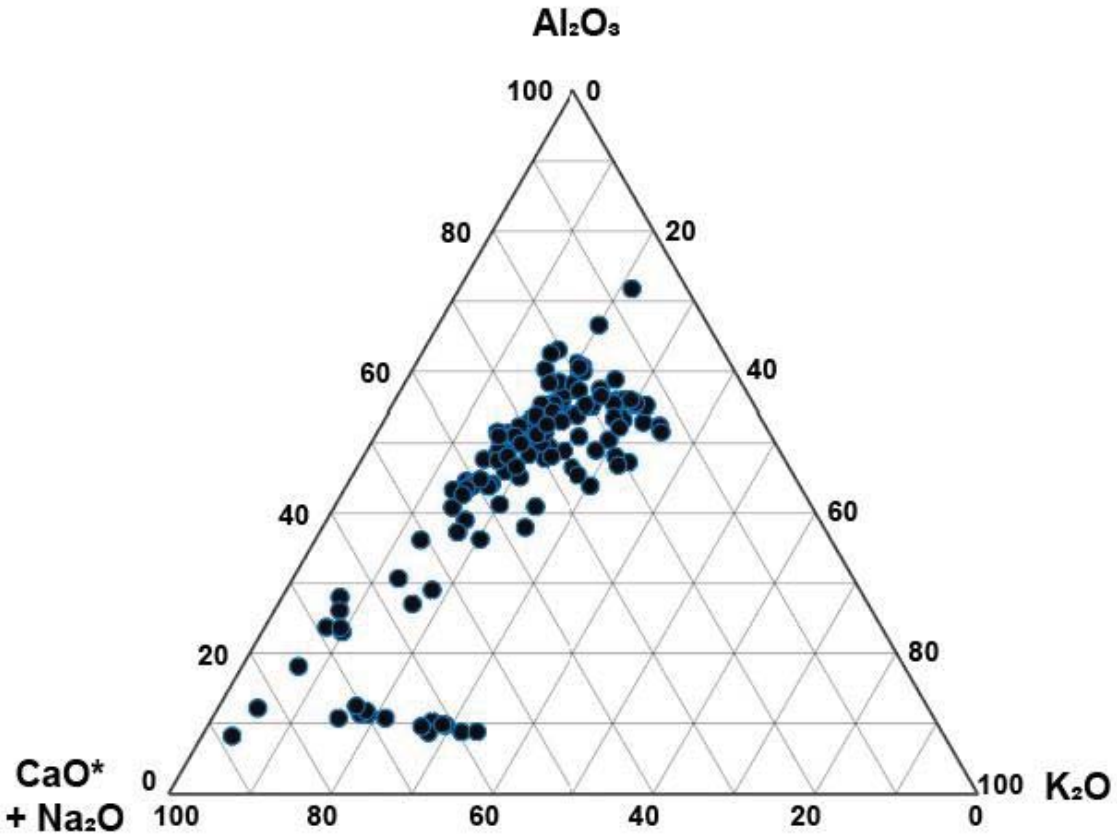

Figure S2. Ternary diagram for all clay samples with available data, showing the relative mole fractions of $CaO+Na_2O$, K_2O, and Al_2O_3.

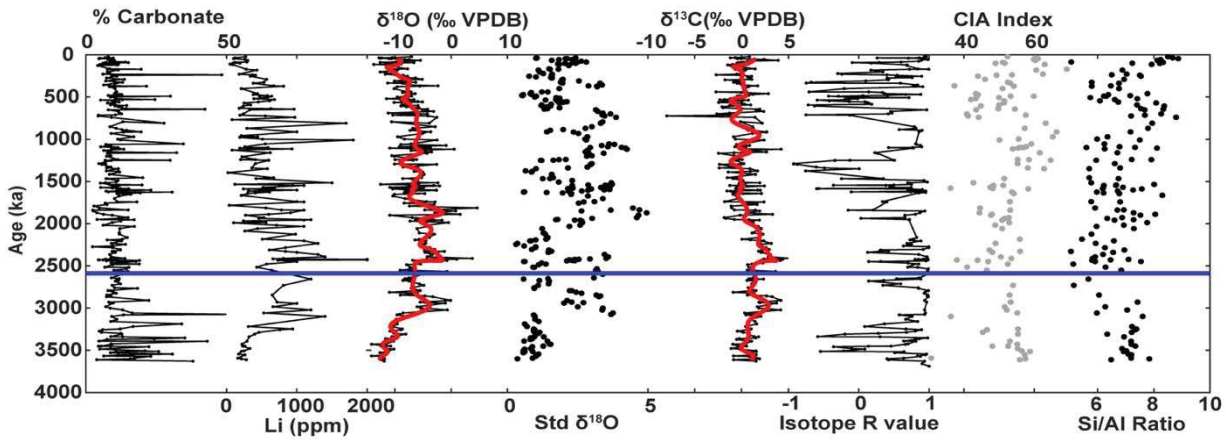

182

183 **Figure S3.** Timeseries from the Clayton Valley EXP2 core. From left to right: percent carbonate;

184 bulk sediment lithium concentrations (ppm); carbonate $\delta^{18}O$ (‰ VPDB); 5 point running

185 carbonate $\delta^{18}O$ standard deviation; carbonate $\delta^{13}C$ (‰ VPDB); correlation coefficient between

186 oxygen and carbon isotopes with a moving window of 10 data points; chemical index of

187 alteration; and Si/Al ratio. Solid red lines are a low pass filtered curve on the carbonate $\delta^{18}O$ and

188 $\delta^{13}C$ records.

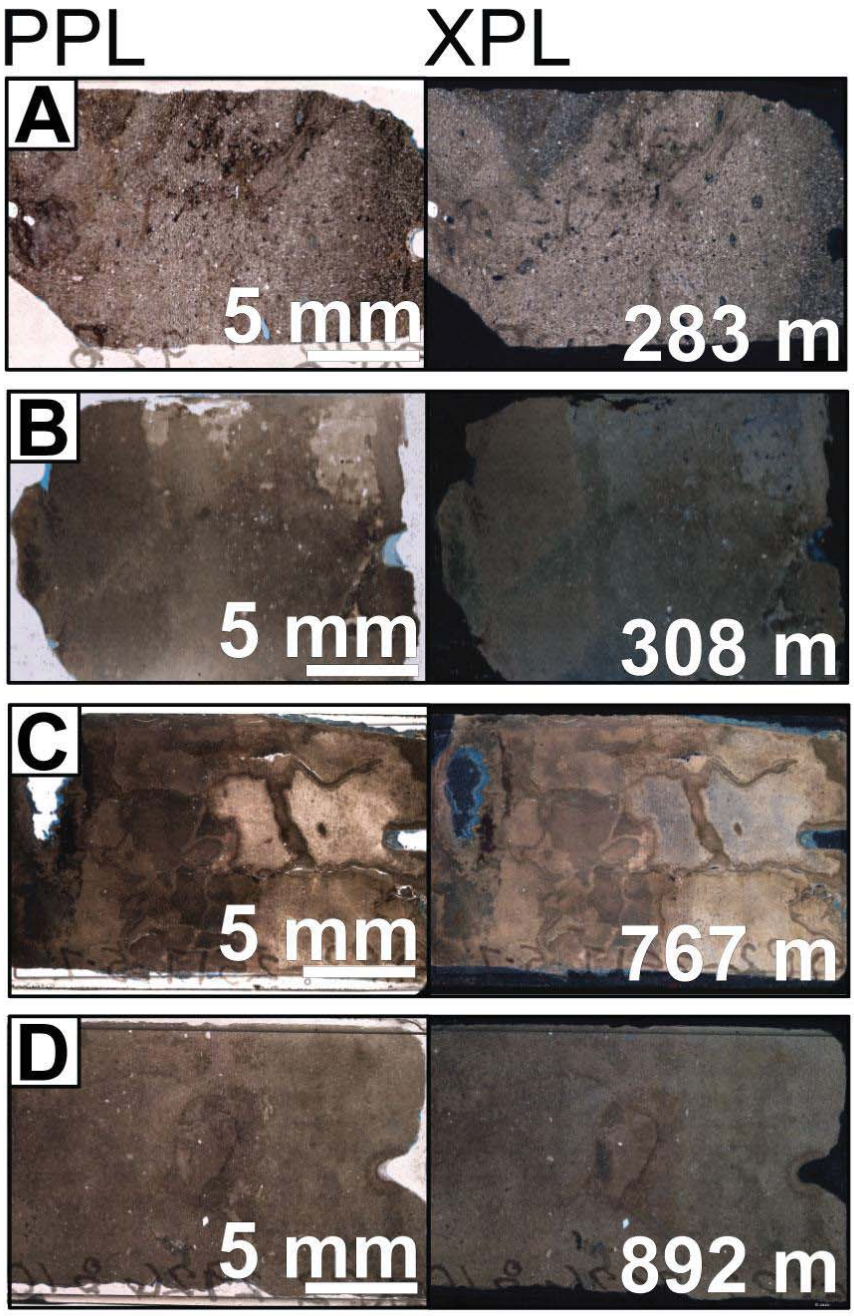

Figure S4. Photomicrogaphs of select lacustrine carbonate intervals from the EXP2 core in plane polarized light (PPL) and cross-polarized light (XPL) showing rare mixed clastic-carbonate intervals (A,D) and micritic text with limited porosity (B-D). Scale bar (5 mm) is displayed on PPL image and core depth in meters is displayed on XPL image.

Supplemental References

Coffey, D. M., Munk, L. A., Ibarra, D. E., Butler, K. L., Boutt, D. F., & Jenckes, J. (2021). Lithium Storage and Release from Lacustrine Sediments: Implications for Lithium Enrichment and Sustainability in Continental Brines. *Geochemistry, Geophysics, Geosystems*, e2021GC009916.

Jicha, B. R., Singer, B. S., & Sobol, P. (2016). Re-evaluation of the ages of 40Ar/39Ar sanidine standards and supereruptions in the western US using a Noblesse multi-collector mass spectrometer. *Chemical Geology*, *431*, 54-66.

Knott, J. R., Machette, M. N., Wan, E., Klinger, R. E., Liddicoat, J. C., Sarna-Wojcicki, A. M., ... & Weamer, V. M. (2018). Late Neogene–Quaternary tephrochronology, stratigraphy, and paleoclimate of Death Valley, California, USA. *Bulletin*, *130*(7-8), 1231-1255.

Knott, J. R., Wan, E., Deino, A. L., Casteel, M., Reheis, M. C., Phillips, F. M., ... & Nunez, E. (2019). Lake Andrei: A pliocene pluvial lake in Eureka Valley, eastern California. *From Saline to Freshwater: The Diversity of Western Lakes in Space and Time, S. Starratt and MR Rosen, Eds*, *536*, 125-142.

Lee, J. Y., Marti, K., Severinghaus, J. P., Kawamura, K., Yoo, H. S., Lee, J. B., & Kim, J. S. (2006). A redetermination of the isotopic abundances of atmospheric Ar. *Geochimica et Cosmochimica Acta*, *70*(17), 4507-4512.

Min, K., Mundil, R., Renne, P. R., & Ludwig, K. R. (2000). A test for systematic errors in 40Ar/39Ar geochronology through comparison with U/Pb analysis of a 1.1-Ga rhyolite. *Geochimica et Cosmochimica Acta*, *64*(1), 73-98.

Mix, H. T., Rugenstein, J. K. C., Reilly, S. P., Ritch, A. J., Winnick, M. J., Kukla, T., & Chamberlain, C. P. (2019). Atmospheric flow deflection in the late Cenozoic Sierra Nevada. *Earth and Planetary Science Letters*, *518*, 76-85.

Paton, C., Hellstrom, J., Paul, B., Woodhead, J., Hergt, J., 2011. Iolite: freeware for the visualisation and processing of mass spectrometric data. *J. Anal. At. Spectrom*. 26, 2508-2518. http://dx.doi.org/10.1039/c1ja10172b.

Reheis, M. C., Sarna-Wojcicki, A. M., Burbank, D. M., & Meyer, C. E. (1991). The late Cenozoic section at Willow Wash, west-central California—a tephrochronologic rosetta stone. *Late Cenozoic stratigraphy and tectonics of Fish Lake Valley, Nevada and California: US Geological Survey Open-File Report*, *91*(290), 46-66.

Reheis, M. C., Slate, J. L., Sarna-Wojcicki, A. M., & Meyer, C. E. (1993). A late Pliocene to middle Pleistocene pluvial lake in Fish Lake Valley, Nevada and California. *Geological Society of America Bulletin*, *105*(7), 953-967.

Sarna-Wojcicki, A. M. (2005). *Tephra layers of Blind Spring Valley and related upper Pliocene and Pleistocene tephra layers, California, Nevada, and Utah: isotopic ages, correlation, and magnetostratigraphy* (No. 1701). US Department of the Interior, US Geological Survey.

Vermeesch, P., 2018, IsoplotR: a free and open toolbox for geochronology. *Geoscience Frontiers*, v.9, p.1479-1493, doi:10.1016/j.gsf.2018.04.001.